ELSEVIER

Sensors and Actuators A 89 (2001) 56–63

SENSORS AND ACTUATORS A PHYSICAL

www.elsevier.nl/locate/sna

A micropolysilicon high-angular-rate sensor with off-chip wireless transmission

Wen J. Li[a,*], Tao Mei[b], Winston Sun[a]

[a]*Department of Automation and Computer-Aided Engineering, The Chinese University of Hong Kong, Shatin NT, Hong Kong*
[b]*Institute of Intelligent Machines, Chinese Academy of Sciences, Hefei, PR China*

Abstract

A novel surface-micromachined, non-contact, high-speed rotation sensor with total surface area under 4 mm^2 was developed using the Multi-User MEMS Processes (MUMPs). This paper reports the initial characterization of the sensor, including rotation and vibration tests. Initial results indicate that this piezoresistive sensor is capable of wirelessly measuring rotation speeds at ~2 Hz/rpm/V with 5 V input in the 100–6000 rpm rotation range. We believe our groundwork will allow the MEMS community to use the MUMPs foundry service to design simple and reliable high-speed rotation sensors that can be interfaced with commercial wireless chips for signal transmission.

Keywords: Non-contact rotation sensing; High-speed rotation sensing; Microrotation sensor; Wireless sensor

1. Introduction

Tachometers have been widely used to measure angular speeds of rotating objects. In general, contact mechanical-based instruments such as handheld tachometers, although capable of giving measurements conveniently as no mounting of extra component is needed, are less accurate than AC or DC electromagnetic-based tachometers. Nevertheless, each type has its own advantages and shortcomings, depending on the applications [1,2]. Optical tachometers are also available that give relatively accurate readings with wide rpm range [3]. However, Kwa and Wolffenbuttel [4] pointed out that some optical sensors are quite sensitive to background light and contamination.

Recently, many new sensor devices based on different non-contact principles, including magnetic field [5], Faraday induction [6], and capacitive [7] were built. However, these devices are generally less reliable than optical sensors because environmental magnetic or electric fields could affect their performances. These techniques also impose restrictions on the material properties or geometry of the rotational components to be measured, and they limit the effective measurable rotation speed. In addition, all these sensors must be accompanied with a stationary reference, which is externally mounted to the systems' housing for proper operation.

We propose to build a MEMS rotation sensor with no externally mounted reference and could be potentially integrated with wireless transmission electrical circuitry. Since these micromachined sensors will be small, they could potentially be embedded into rotating objects such as gears or shafts. Many MEMS motion sensors have been fabricated using piezoelectric, piezoresistive, or capacitive principles [8–10]. Nonetheless, the existing sensors are designed mainly for low-angular speeds (i.e. <1000 rpm) and acceleration measurements. In addition, to the best of our knowledge, no high-speed rotation sensors were built using the MCNC commercial foundry (renamed to CRONOS Integrated Microsystems Inc.) and have wireless transmitted output.

Various groups are developing either microcomponents for wireless communication or using wireless transmission method for their microsensors. For example, GIT [11], UCLA [12], University of Michigan [13], and University of Tennessee [14] have ongoing wireless related MEMS projects. However, to the best of our knowledge, no one has yet presented work on merging commercial wireless chips with foundry fabricated high-speed rotation sensors. Our developed sensors offer a reliable, non-contact, no off-mounted reference technique to high-speed rotation sensing along with other benefits of MEMS technology. And, unlike the existing MEMS motion sensors that could be used for rotation measurement, but which are usually

* Corresponding author. Tel.: +852-2609-8475; fax: +852-2603-6002.
E-mail address: wen@acae.cuhk.edu.hk (W.J. Li).

0924-4247/01/$ – see front matter
PII: S0924-4247(00)00542-2

optimized for low-speed sensing and are more complex in design, the sensor we report here has a simple design which can be foundry fabricated, and therefore, viable for commercialization.

This paper presents the design, analysis, and initial experimental results of polysilicon cantilever rotation sensors that can measure angular speeds between 100 and 6000 rpm. These sensors are designed to have small size, low power consumption, low cost, wide dynamic range, and yet accurate. For demonstration, we have used the MUMPs foundry to fabricate the mechanical elements that were then interfaced with commercial wireless transmission chips.

2. Sensor concept and design

The concept for measuring rotation speed of a spinning body using embedded microsensors is illustrated in Fig. 1. A three-dimensional illustration of a sensor is shown in Fig. 2. The oxide layer underneath the mass platform and the supporting polysilicon cantilevered beams was sacrificially etched using hydrofluoric acid and critical CO_2 drying process by MCNC. Etch holes were needed to provide shorter release etch paths under the mass platform which is supported by two polysilicon cantilevers and is freed for deflection by centrifugal force. A scanning electron microscope (SEM) picture of a pair of the surface-micromachine sensors is shown in Fig. 3. The mass platforms are sacrificially released and are curved due to residual stresses between different thin film layers in this case. Three MUMPs thin film layers which make up the platforms are apparent in this picture: Poly 1, Poly 2, and Au. A reference sensor structure that was not sacrificially released is shown in Fig. 4. An interferometric image showing the curvature of a sacrificially released mass platform in both transverse and axial directions is shown in Fig. 5.

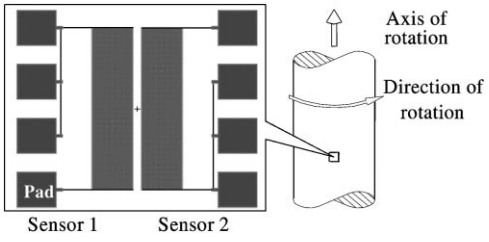

Fig. 1. Conceptual drawing of microsensors embedded in rotating structures to measure rotation (not to scale).

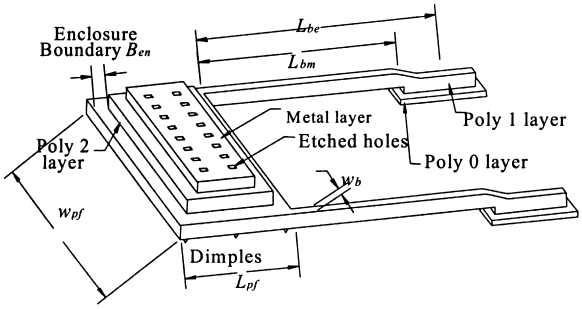

Fig. 2. Three-dimensional drawing of a surface-micromachined rotation sensor using polysilicon as cantilever beams supporting a multi-layered mass platform.

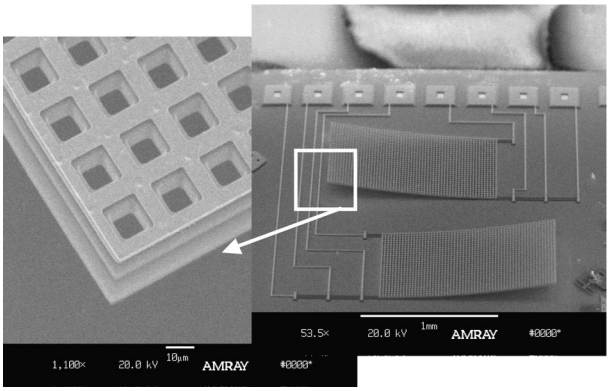

Fig. 3. SEM picture of a pair of fabricated sensors. The curvature of the mass plate is due to residual stress between different layers of materials making up the plate.

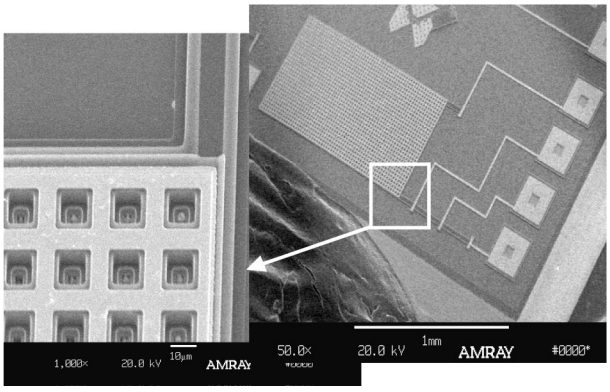

Fig. 4. SEM picture of a reference sensor. MUMPs layers shown in the SEM include Poly 0, Poly 1, Poly 2, and Au.

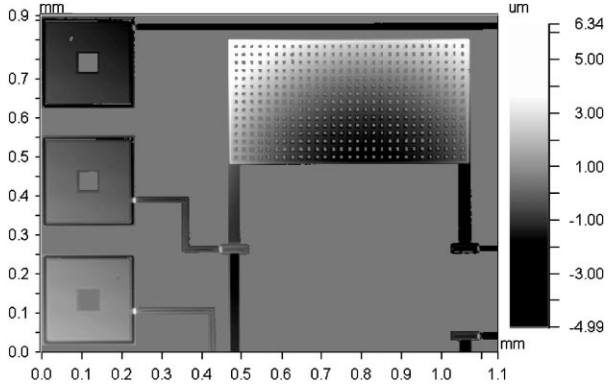

Fig. 5. Interferometric image of a surface-micromachined rotations sensor.

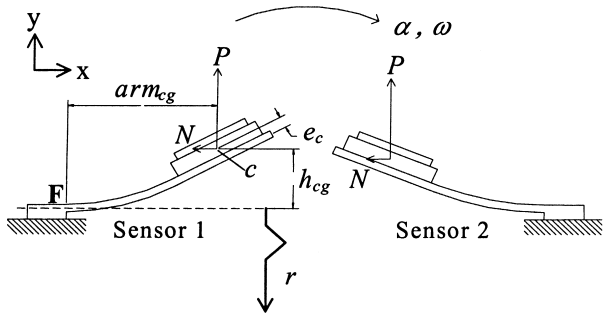

Fig. 6. This illustration shows a pair of rotation sensors. The design parameters are also shown in this figure.

2.1. Theoretical analysis

As shown in Fig. 6, a set containing two identical sensors in opposite directions is oriented so that the axes of the cantilevered beams are perpendicular to the axis of rotation. As will be discussed later, a set of two sensors can be used to measure the angular acceleration of the rotating element.

If no linear motion exists along the rotation axis then lateral deflection of the beams, or transverse stress, can be neglected. Excluding the substrate, a MCNC fabricated sensor is less than 5.1 μm thick (platform) and weighs about 3–15 μg theoretically, depending on the platform size. As shown in Fig. 6, the initial moment arm from the centroid c to the fixed end F is a constant. When centrifugal force is induced on the seismic mass by an angular velocity (ω) or acceleration (α), the length of this moment arm will change. Also, the vertical load $P = mr\omega^2$ induced by rotation and the axial load $N = mr\alpha$ caused by angular acceleration (r is the distance from the axis of rotation to the neutral axis of the cantilever) both act on the centroid c of the platform. The distance e_c is a constant with its value dependent on the number of polysilicon layers. It is measured from the centroid of the platform to the neutral axis of the beam. The maximum strain on the cantilever beams occurs at F, the fixed end of the beams. From Fan et al. [15] the maximum allowable strain of polysilicon is about 1.7%. At $t > 0$ s, the platform will be raised by a distance h_{cg} due to centrifugal force. Consequently, the beams are under stress and deformed in a curved shape. The beams will also undergo slight elongation or shortening, depending on the combined effect of P and N. The moment arm measured from the fixed end F to the centroid will also be shifted from initial distance to arm_{cg}.

The governing differential equation for the bending beam is shown in Eq. (1) below. The moment and stress equations are shown in Eqs. (2) and (3), respectively.

$$EI\frac{\mathrm{d}^2 y_i}{\mathrm{d}x_i{}^2} + Px \pm Ny - M_i = 0 \tag{1}$$

$$M_i = P\text{arm}_{cg} \pm Nh_{cg} \tag{2}$$

$$(\sigma_{net})_i = -\left(\frac{M_i t(f-1)}{6I_w} \pm \frac{N}{A_{bm}}\right), \quad i = 1,2 \tag{3}$$

The index i denotes sensors 1 and 2 in Fig. 6. In Eq. (3), I_w is the moment of inertia of the trapezoidal cross-sectional area about the neutral axis, f the wedge factor and is the ratio of beam-center-width to beam-bottom-width, t the beam thickness, and A_{bm} the total cross-section area of the two combined beams. The neutral axis is not at $t_{bm}/2$ for MCNC fabricated beams due to the fabrication process which causes the beams to have a trapezoidal cross-section. Eq. (2) is obtained by summing the moments about any arbitrary point (x_i, y_i) along beam i. Analytical solutions of Eq. (1) can be readily obtained from symbolic mathematical packages (e.g. Mathematica) for a given set of values of r, ω and α. For transient calculations, the results of Eq. (1) could be used to obtain arm_{cg} and h_{cg} at a given time, which could then be used in Eq. (2) to obtain a more accurate solution. Finally, the results of Eq. (2) could be substituted into Eq. (3) to find the stress profile in the beam.

The deflection or elongation of the beams causes a change of resistance of the polysilicon, which could be converted into a measurable change of voltage by connecting the sensors in a Wheatstone bridge configuration [16]. The change of resistance due to beam elongation could then be expressed as a function of gauge factor G [17] as shown in Eq. (4)

$$\frac{\Delta R_i}{R} = \frac{G}{L_{bm}}\int_0^{L_{bm}} \frac{\sigma_i}{E}\,\mathrm{d}x \tag{4}$$

where R is the total resistance of the sensor and is typically about 10 Ω/sq for polysilicon [18], σ_l the longitudinal stress in Eq. (3), and σ_t the transverse stress which can be neglected at steady state conditions. When a steady state rotational speed is achieved, axial load N tends to zero, and the two sensors will have the same deflection and change of resistance. However, when the angular acceleration α is $\gg 0$, such as during motor startup or under sudden change of speed, the transient response of sensor 1 and sensor 2 will be different due to the contribution from N. Hence, by monitoring the transient response of the sensors, the direction of acceleration could be determined. We have used the above theoretical analysis in designing the sensors to measure angular speeds up to 8000 rpm.

3. Experimental results

Each MCNC run gave us 15 chips that have 10 rotation sensors and other devices designed for our various on-going projects. We have measured the change of resistance due to bending of the piezoresistive polysilicon cantilever beams for sensors of different designed parameters on different MCNC chips. Table 1 is a representative comparison of sensor designs with different cantilever widths (W), lengths (L), and platform sizes. In the table, f denotes failure of the beams due to excessive strain at the given deflection angle. The deflection angle is the angle between the tip of the mass

Table 1
Deflection of the platform varies with cantilever dimensions

Deflection angle	Platform size (600 μm × 320 μm)				Platform size (600 μm × 1200 μm)					
	$W = 30$ μm, $R_3 = 154.9\ \Omega$		$W = 14$ μm, $R_3 = 266.75\ \Omega$		$W = 20$ μm, $R_3 = 223.15\ \Omega$		$W = 30$ μm, $R_3 = 146.64\ \Omega$		$L = 200$ μm, $W = 20$ μm, $R_3 = 369.05\ \Omega$	
	ΔR_3 (Ω)	(%)	ΔR_3 (Ω)	(%)	ΔR_3 (Ω)	(%)	ΔR_3 (Ω)	(%)	ΔR_3 (Ω)	(%)
25	0.474	0.306	1.364	0.511	0.866	0.388	0.489	0.333	0.765	0.207
35	0.852	0.550	2.687	1.007	1.566	0.702	0.778	0.531	1.190	0.322
45	1.292	0.834	3.963	1.486	2.407	1.079	1.157	0.789	1.843	0.499
55	f	f	5.486	2.057	3.467	1.554	1.620	1.105	2.518	0.682

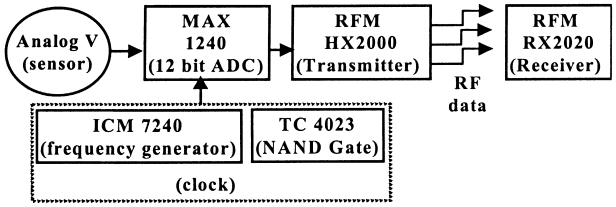

Fig. 7. Block diagram for digital transmission of sensor data. Sensor data is digitized before RF transmission.

platform and the substrate. The resistance change typically varies from 0.5 to 2% as shown in the table.

3.1. Wireless transmission chips

Commercial wireless transmitters and receivers which could be eventually interfaced with our rotation sensors were evaluated for signal transmission. Two basic configurations were evaluated. The first configuration, as shown in Fig. 7, maps the analog voltage output from the sensor into digital data before RF transmission by the transmitter. The volume of the entire transmitter circuitry, including the sensor, battery, and IC chip packaged ADC, clock, and RF transmitter is about 1 cm × 3 cm × 3 cm. When the ADC, clock, and RF transmitter die are used instead of the IC packaged chips, the entire transmitter circuitry should be significantly smaller. A second type of transmission scheme, which maps the voltage from a sensor into frequency before the RF transmission, is shown in Fig. 8. The overall volume of the IC packaged chips for this scheme is only 1/3 the size of the previous method but a frequency counter must be used at the receiver end to decipher the original voltage information.

We have adopted the second configuration at this time because it is simpler to build and has a good transmission performance experimentally. However, we have found that the TX2 transmitter (Radiometrix) works better than the HX2000 (RFM) for our sensors. The circuit configuration is implemented as shown in Fig. 9. The change of resistance across the bending beams (ΔR_3) is transduced into a change of differential voltage and then amplified by the AMP04 instrumentation amplifier, which has an adjustable gain between 1 and 1000. The amplified voltage is then converted into frequency signal by an AD654 voltage-to-frequency converter. This stage is essential for the TX2 transmitter to provide stable signal transmission. The potentiometer at R_4 could be adjusted such that variation of bridge output is beyond the initial offset and within the linear region of

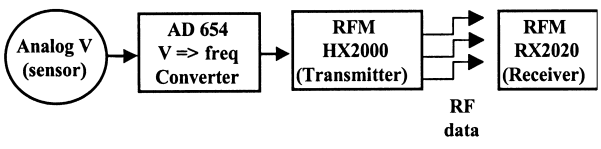

Fig. 8. Block diagram for digital transmission of sensor data where the sensor data is mapped to a frequency domain before transmission.

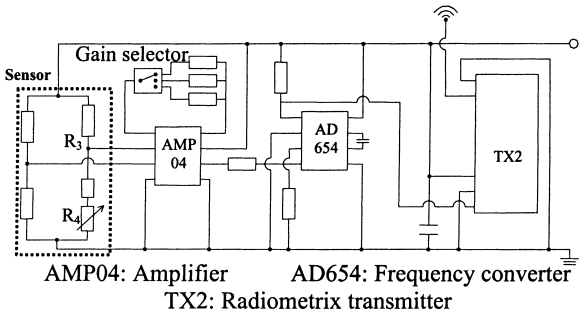

Fig. 9. Schematic drawing of the wireless transmission circuit system which is used to transmit the surface-micromachined sensor.

AMP04 as well as bounded by the upper frequency limit of TX2 at around 28 kHz (carrier frequency of 433 MHz). The signal is detected wirelessly by the Radiometrix RX2 (not shown in the figure).

3.2. Experimental setup

The conceptual drawing and a picture of the actual experimental setup to measure rotation speeds of a disk are shown in Fig. 10. The rotating disk is replaceable in our design. The power supply, and the wireless data transmission chips are placed within a small package made by a CNC plastic injection machine, which is then placed on the rotating disk.

3.3. Sensor results

The MCNC fabricated sensors were tested for piezoresistivity by using probes to lift the platforms while measuring changes in resistance across the beam-platform-beam connection (Fig. 1). The variations of resistance versus deflection angle of the platform from the substrate for several sensor designs are shown in Fig. 11. Although the variations are non-linear they are very consistent. As predicted by theory, narrower beams give higher resistance change and are prone to structural failure at higher deflection angles. For instance, 14 μm × 100 μm beams will fail at ∼60° while 20 μm × 200 μm and 30 μm × 200 μm beams will survive beyond deflections angles of ∼80° as shown in Fig. 11. The circuit shown in Fig. 9 was calibrated using a potentiometer that has a nominal value close to R_3 (resistance of a designed sensor). The frequency output of the AD654 versus the change of the potentiometer (R_4) is linear over ∼20% change of resistance (which gives a linear output frequency between 10 and 25 KHz). Each moving-platform sensor was connected to two integrated polysilicon resistors on chip and a potentiometer off-chip to form a Wheatstone bridge. The bridge output was connected via wirebonding to pads on a PCB that contains the signal transmission circuitry. Typical frequency output received by the RX2 receiver as the sensor is rotated is shown in Figs. 12 and 13. The response of the sensor, as shown in Fig. 12, is non-linear as

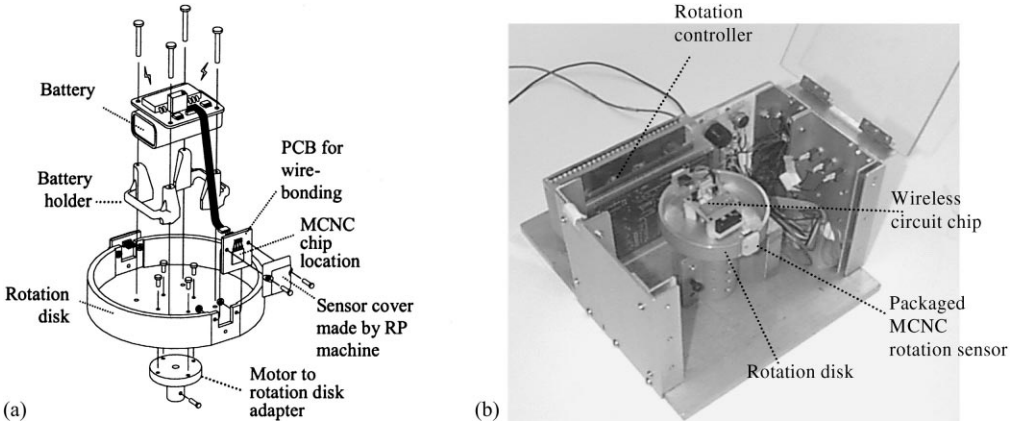

Fig. 10. (a) Conceptual drawing and (b) actual picture of the experimental rotating disk packaged with wireless rotation MEMS sensor.

predicted since the supporting cantilevered beams underwent large deflections over the dynamic range tested.

The small-deflection beam theory does not hold for the entire sensor dynamic range, and hence, strains on the beams are not linearly proportional to the deflection. However, as indicated in Fig. 13, for lower rotation speeds, the linear theory will hold, and the output of the bridge is proportional to V^2/R_d, where V is the tangential velocity of the rotating disk, and R_d the radius of the disk.

We have also developed an ANSYS model for the sensor structure to check the theoretical formulation derived in Eqs. (1)–(3). ANSYS modeling will also allow us to predict sensor performance for more complex structural designs. Comparison of an ANSYS sensor-model result with the theoretical results from Eqs. (1) and (2) is shown in Fig. 14. The results agree closely as shown and, consequently, will allow us to (1) use Eqs. (1) and (2) to design and predict the performance of simple cantilever-platform sensors; (2) use ANSYS to determine the total piezoresistivity change of the sensor structure more accurately to include three-dimensional effects on the strain of the sensor structure; (3) use ANSYS to design other sensor structures. Note, however, that the non-linear bending of the beams are not predicted by Eqs. (1) and (2) nor modeled by our ANSYS model.

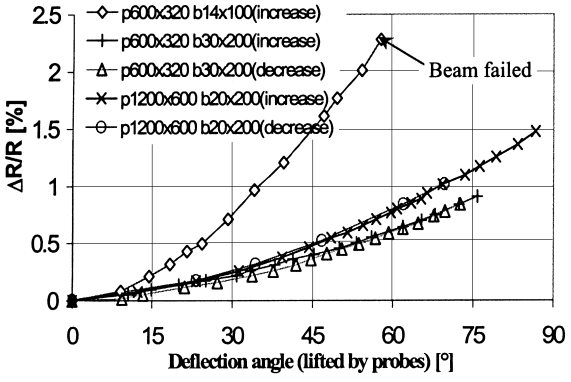

Fig. 11. Change of resistance as a function of beam deflection.

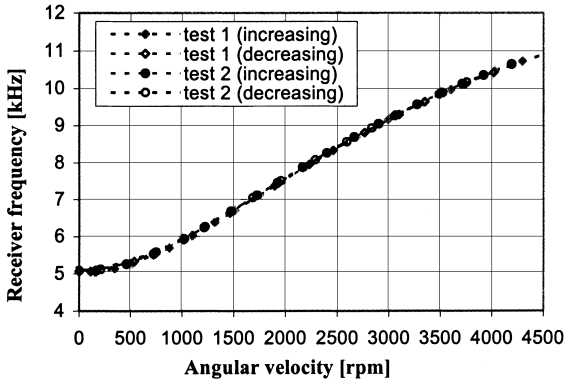

Fig. 12. Wireless transmitted data from a rotation sensor. The sensor has a 1200 μm × 600 μm platform supported by 20 μm × 100 μm beams, and was rotated on a 10 cm disk. Some sensors were tested up to 6000 rpm before beam failure.

We have also attempted to predetermine the received frequency in the wireless transmission circuit versus given rotation speeds using Eqs. (1)–(4) (if the electronic gains are known a priori). However, Eqs. (1) and (2) have assumed small and linear deflection in their formulation, hence cannot predict the frequency output accurately for the entire experimental dynamic range, since the sensor structures will under go large and non-linear deflections at high speeds.

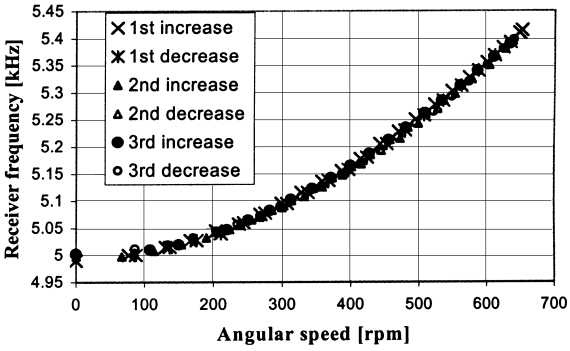

Fig. 13. Wireless transmitted data from a sensor rotated at below 1000 rpm (same sensor as Fig. 12). Sensor response to angular rotation at lower speeds is different from at higher speeds.

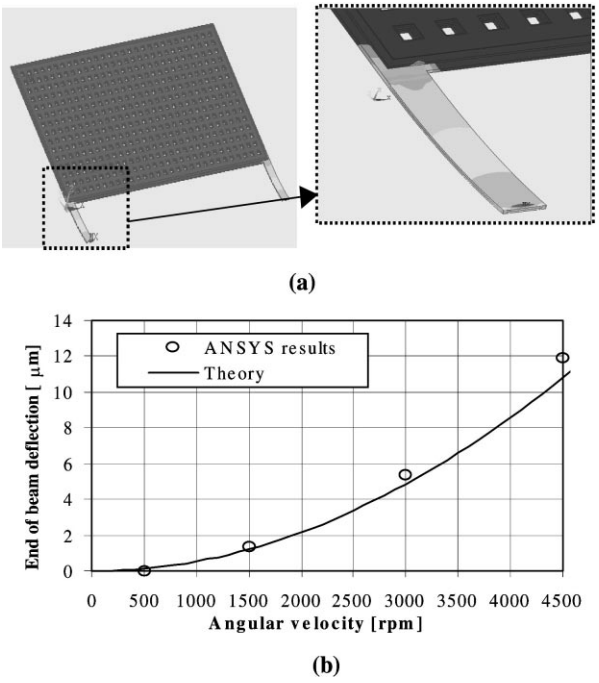

Fig. 14. (a) ANSYS model of a rotation sensor and (b) comparison of theoretical and ANSYS results for deflection of a sensor on a 10 cm disk rotated up to 4500 rpm. The structure analyzed has a 600 μm × 320 μm platform with beam dimensions of 20 μm × 100 μm.

If Eq. (4) is replaced with experimental data for resistance change versus deflection as given in Fig. 11, then the prediction will be much more accurate. This comparison is shown in Fig. 15.

We have also subjected the sensors to the frequency and amplitude vibration range shown in Fig. 16. The sensors have all survived vibrations in both longitudinal and lateral directions in the range given in the figure. Experiments to test the temperature dependence and power consumption of the sensors were also conducted. The resistance of the sensors, which compose of a multi-layered platform and

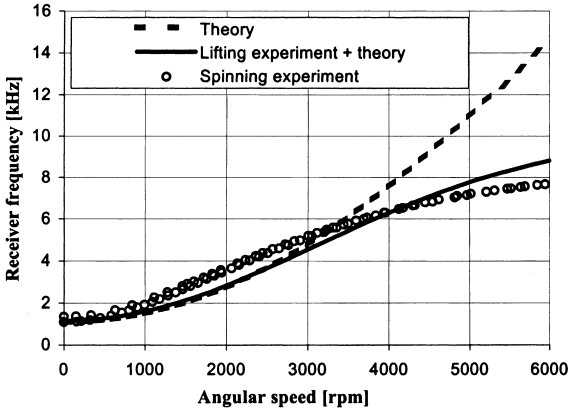

Fig. 15. Comparison of experimental, theory, and theory plus lifting-experiment results. The theory under predicts sensor output at lower rpms possibly due to two factors: (1) piezoresistive change of the mass platform and (2) aerodynamic lifting of the mass platform.

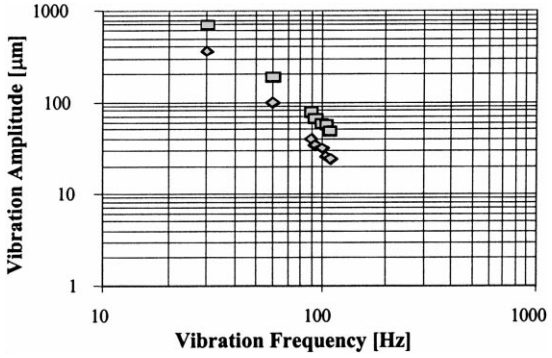

Fig. 16. Amplitude versus frequency of the vibration used to test the sensors.

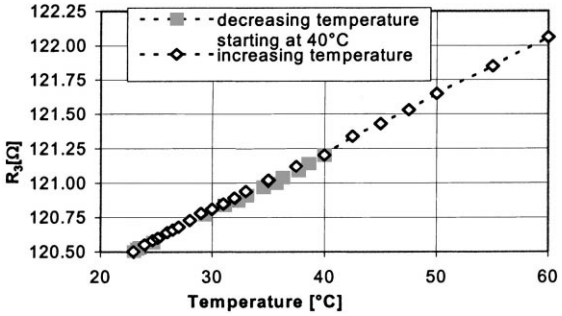

Fig. 17. Temperature dependence of a typical polysilicon cantilever rotation sensor.

two polysilicon cantilevers, varies linearly with temperature fluctuations in the range shown in Fig. 17. Power consumption for the sensors was also analyzed. An *I–V* curve for a typical sensor is shown in Fig. 18. We are presently operating the sensor with 5 V input which corresponds to ∼0.2 W of power. However, as indicated in the figure, with 5 V input the sensor structure will undergo resistive-heating, causing the non-linear *I–V* relationship, and hence, 5 V is probably not the ideal operation input voltage. We are currently analyzing the relationship between input voltage, power consumption, and sensitivity of the high-speed rotation sensors.

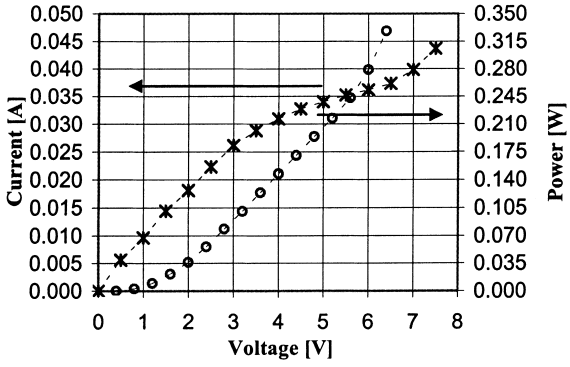

Fig. 18. Power consumption of a typical rotation sensor. Power is calculated by the product of current and voltage.

4. Conclusion

The design of a novel surface-micromachined rotation sensor is presented. It is designed to detect the angular velocity of a rotating element by measuring the resistance change due to stress induced by centrifugal force on the seismic mass using piezoresistive effects. The designed sensors were fabricated using the MUMPs-29 run. Several wireless transmission schemes for the rotation sensors were evaluated and we have selected the Radiometrix TX2 transmission chip for our experiments. Experimental results showed a 13 μg platform proof-mass could be used to detect rotation speeds of 100–6000 rpm if appropriate structural designs are implemented. We will further improve the rotation sensing system by interfacing it with low power wireless systems and also test the feasibility of using a pair of co-located structures for angular acceleration detection.

Acknowledgements

We would like to thank Mr. Tin-Tak Tsang for contributing to the test and analysis of various commercial wireless transmission schemes. This work was funded by the Chinese University of Hong Kong Research Direct Grant (#2050173) and the Hong Kong Information Technology Entrepreneur Programme.

References

[1] J.A. Haslam, G.R. Summers, D. Williams, Engineering Instrumentation and Control, Edward-Arnold, London, 1981, p. 133.
[2] C.L. Nachtigal, Instrumentation and Control — Fundamentals and Applications, Wiley, New York, 1990, pp. 370.
[3] R.C. Spooncer, A.S. Nicholson, M.R. Oliver, An optical tachometer with optical fibre links, IEE Colloquium on IREM, London, UK, 1991.
[4] T.A. Kwa, R.F. Wolffenbuttel, An integrated high-resolution optical angular displacement sensor, IEEE Transducers'91, San Francisco, USA, 24–27 June, 1991.
[5] K. Watanabe, C. Kim, Non-contact revolution measurement by the magnetic field intensity from axes, IEEE IMTC'94, Hamamatsu, Japan, 10–12 May, 1994.
[6] A. Powell, T. Meydan, Optimization of magnetic speed sensors, IEEE INTERMAG'96, Seattle, Washington, USA, 9–12 April, 1996.
[7] T. Fabian, G. Brasseur, A robust capacitive angular speed sensor, IEEE IMTC'97, Ottawa, Canada, 19–21 May, 1997.
[8] J. Söderkvist, Piezoelectric beams and angular rate sensors, in: IEEE Proceedings on the 44th Annual Symposium on Frequency Control, Baltimore, MD, USA, 23–25 May, 1990.
[9] A.M. Madni, L.A. Wan, S. Hammons, A microelectromechanical quartz rotational rate sensor for inertial applications, in: IEEE Aerospace App. Conference, Aspen, CO, USA, 3–10 February, 1996.
[10] R. Voss, K. Bauer, W. Ficker, T. Gleissner, W. Kupke, M. Rose, S. Sassen, J. Schalk, H. Seidel, E. Stenzel, Silicon angular rate sensor for automotive applications with piezoelectric drive and piezoresistive read-out, IEEE Transducers'97, Chicago, USA, 16–19 June, 1997.
[11] J.M. English, M.G. Allen, Wireless micromachined ceramic pressure sensors, IEEE MEMS'99, FL, USA, 17–21 January, 1999.
[12] W.J. Kaiser, K. Bult, A. Burstein, D. Chang, Wireless integrated microsensors, in: Proceedings of the Tech. Dig. of the 1996 Solid State Sensor and Actuator Workshop, Hilton Head Island, SC, USA, 1996, pp. 205–210.
[13] C.T.-C. Nguyen, Microelectromechanical devices for wireless communications, IEEE MEMS'98, Heidelberg, Germany, 25–29 January, 1998.
[14] C.L. Britton, R.J. Warmack, S.F. Smith, P.I. Oden, R.L. Jones, T. Thundat, G.M. Brown, W.L. Bryan, J.C. Depriest, M.N. Ericson, M.S. Emery, M.R. Moore, G.W. Turner, A.L Winterberg, T.D. Threatt, Z. Hu, L.G. Clonts, J.M. Rochelle, Battery-powered, wireless MEMS sensors for high-sensitivity chemical and biological sensing, in: IEEE Proceedings of the 20th Annual Conference on Advanced Research in VLSI, AL, USA, 21–24 March, 1999.
[15] L.S. Fan, Y.C. Tai, R.S. Muller, Integrated movable micromechanical structures for sensors and actuators, IEEE Trans. Electron Devices ED-35 (1988) 724–730.
[16] T.G. Beckwith, R.D. Marangoni, Mechanical Measurements, 3rd Edition, Addison-Wesley, 1982, p. 134.
[17] B. Kloeck, in: W. Göpel, J. Hesse, J.N. Zemel (Eds.), Sensors — A Comprehensive Survey, Vol. 7, Weinheim, Germany, 1994, pp. 145–172, Chapter 5.
[18] D.A. Koester, R. Mahadevan, B. Hardy, K.W. Markus, MUMPs Design Handbook, Rev. 5.0, CRONOS Integrated Microsystems, 2000.